Visualizing the dynamic metallation state of NDM-1 in bacteria using a reversible fluorescent probe

Radhika Mehta,[a] Dann D. Rivera,[b] David J. Reilley,[c] Pei W. Thomas,[b] Abigail Hinojosa,[a] Dominique Tan,[a] Alesha C. Stewart,[b] Zishuo Cheng,[d] Michael W. Crowder,[d] Anastassia N. Alexandrova,[c] Walter Fast,*[b] Emily L. Que*[a]

[a] Department of Chemistry, University of Texas at Austin, 105 E 24th St Stop A5300, Austin, TX 78712

[b] Division of Chemical Biology & Medicinal Chemistry, College of Pharmacy, University of Texas, Austin, Texas 78712

[c] Department of Chemistry and Biochemistry, University of California-Los Angeles, 607 Charles E. Young Drive, Los Angeles, California 90095-1569

[d] Department of Chemistry and Biochemistry, Miami University, Oxford, Ohio 45056

ABSTRACT: New Delhi Metallo-β-lactamase (NDM) grants resistance to a broad spectrum of β-lactam antibiotics including last-resort carbapenems and is emerging as a global antibiotic resistance threat. Limited zinc availability adversely impacts the ability of NDM-1 to provide resistance, but a number of clinical variants have emerged that are more resistant to zinc scarcity (*e.g.,* NDM-15). To provide a novel tool to better study metal ion sequestration in host-pathogen interactions, we describe the development of a fluorescent probe that reports on the dynamic metallation state of NDM within *E. coli*. The thiol-containing probe selectively coordinates the dizinc metal cluster of NDM and results in a 17-fold increase in fluorescence intensity. Reversible binding enables competition and time-dependent studies that reveal fluorescence changes used to detect enzyme localization, substrate and inhibitor engagement, and changes to metallation state through the imaging of live *E. coli* using confocal microscopy. NDM-1 is shown to be susceptible to demetallation by intracellular and extracellular metal chelators in a live-cell model of zinc dyshomeostasis, whereas the NDM-15 metallation state is shown to be more resistant to zinc flux. The development of this reversible turn-on fluorescent probe for the metallation state of NDM provides a new tool for monitoring the impact of metal ion sequestration by host defense mechanisms and to detect inhibitor target engagement during the development of therapeutics to counter this resistance determinant.

INTRODUCTION

New Delhi Metallo-β-lactamases (NDM) are an emerging global antibiotic resistance threat with the ability to hydrolyze and thereby inactivate almost all clinically used β-lactam drugs, including last-resort carbapenems.[1-2] First identified in 2008,[3] NDM-1 is a dizinc metalloprotein with broad substrate promiscuity encompassing a wide range of penicillins, cephalosporins, and carbepenems.[4-6] The metal cluster is comprised of two zinc ions, with the first (Zn1) coordinated to 3 histidines, the second (Zn2) coordinated to an aspartate, cysteine and histidine, and both zinc ions bridged by a nucleophilic hydroxide ion.[7] The binding constants for each zinc site are quite disparate ($K_{d, Zn1} \sim 1$ nM; $K_{d, Zn2} \sim 1$ μM) when measured using a soluble mutant of NDM-1 that lacks an *N*-terminal lipidation sequence.[8] Characterization of emerging clinical variants of NDM (NDM-1 through NDM-17) revealed that many of these mutations impart enhanced affinity for Zn2 (*e.g.,* NDM-15 $K_{d, Zn2} = 120$ nM), and likely arose due to the dual

selective pressures of antibiotic treatment and zinc scarcity.[8-10] Lipidation of full length NDM-1 tethers the enzyme to the inner leaflet of the outer membrane and increases zinc affinity, but this form of NDM-1 still remains notably more susceptible to ampicillin in the presence of metal chelators than NDM variants with increased Zn2 affinity.[8, 11] The weak affinity of NDM-1 for Zn2 appears to be a vulnerability likely exploited both by infected hosts through nutritional immunity and by design of β-lactam:chelator co-drug strategies.[12-13]

At the host-pathogen interface, nutritional immunity can use metal dyshomeostasis to adversely impact bacterial survival through sequestration of zinc, manganese, iron and other metal ions.[14-17] The metallation of other metallo-β-lactamases is dependent on extracellular metal ion identity and concentration.[18] Resistance imparted by NDM[11, 19] and other multi-drug resistant bacterial systems[20-21] is adversely impacted by chelation of extracellular zinc by the host derived protein calprotectin[11, 20, 22] or
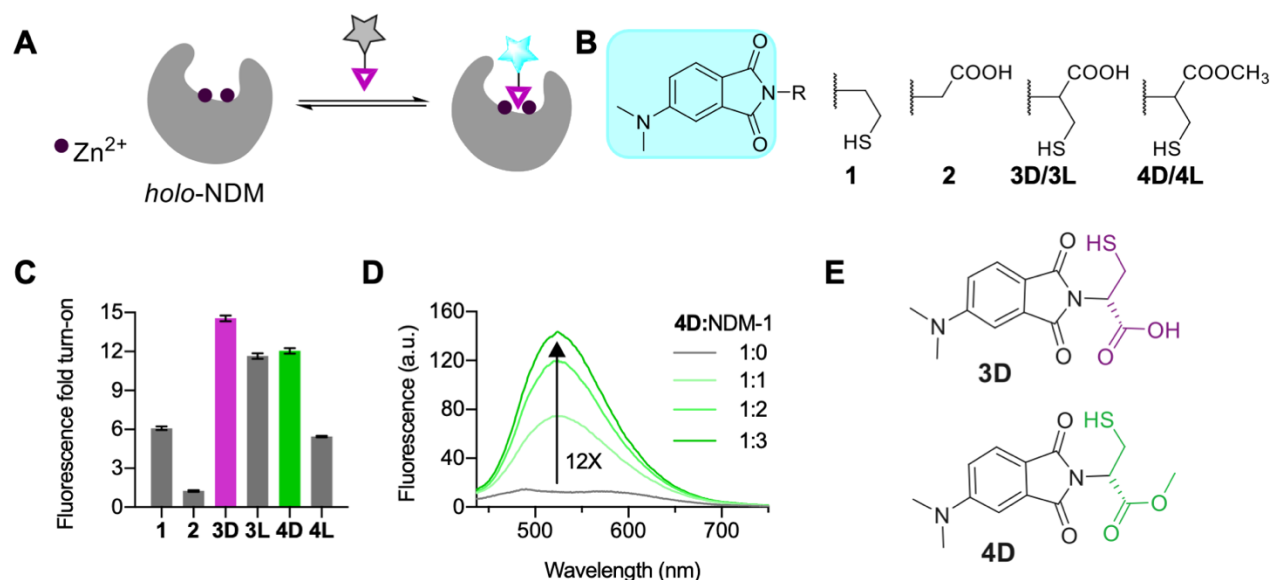
Figure 1. (A) Design of reversible NDM-1 fluorescent probes. (B) Structures of probes 1-4. (C) Fluorescence fold turn-on of probes with NDM-1 (1:3 ratio, 10 μM probe; λ_{ex} = 420 nm). (D) Fluorescence spectra showing the fluorescence turn-on for probe 4D (10 μM) with increasing equivalents of NDM-1. λ_{ex} = 420 nm. (E) Probes showing the best fluorescence response with NDM-1. All studies were conducted in degassed 50 mM HEPES, 10 μM ZnSO$_4$ buffer, pH 7.0 at room temperature using acetonitrile (≤5% v/v) as a cosolvent.

exogenously added small-molecule chelators.[23] However, detecting the metallation state of NDM and its clinical variants during these challenges is not straightforward and usually relies on the use of purified components, or measurements of enzyme activity or bacterial growth. To better study the interplay of nutritional immunity and NDM in antibiotic resistance, we sought to develop a new tool to directly monitor the metallation state of NDM *in situ*.

Previously, we studied models of zinc dyshomeostasis in HeLa cells by designing small molecule fluorescent probes that report on the metallation status of intracellular carbonic anhydrase.[24] Some existing NDM-1 targeted fluorophores consist of fluorogenic substrates[25-26] or covalent modifiers,[27-28] and represent irreversible "switch on" probes. However, these probes do not necessarily report on metallation and lack the ability to monitor dynamic reversible changes. Herein, we developed a reversible fluorescent detector for NDM metallation by coupling an environmentally-sensitive fluorescent reporter to a thiol-containing moiety similar to those contained in previously reported NDM inhibitors.[29-30][31] Thiol-based inhibitors are a well-established inhibitor-type for metallo-β-lactamases in which the thiol displaces the nucleophilic hydroxide ion and forms a new bridge between Zn1 and Zn2.[6] The base of the neighboring substrate-binding β-hairpin loop consists of hydrophobic residues, which contrast with the aqueous solvent and provide a much different environment for the bound fluorophore.[6] Using this approach, we report the development and characteriza-

tion of a reversible fluorescent probe selective for the holo dizinc form (metalloform) of NDM-1 and demonstrate its use with confocal microscopy to visualize the dynamic metallation states of clinical NDM variants in live bacteria when challenged by zinc sequestration agents as a model of nutritional immunity.

RESULTS AND DISCUSSION

Synthesis and photophysical properties of the synthesized probes. To make a fluorescent probe specific for dizinc NDM-1, we linked the environment-sensitive fluorophore, 4-N,N-dimethylaminopthalimide (4-DMAP)[32] with thiol derivatives predicted to bind NDM-1 with micromolar affinity *via* direct interactions with both Zn^{2+} ions in the enzyme active site (Fig. 1). These small molecule fluorescent probes for NDM-1 (Fig. 1B) were synthesized in multiple steps from *N,N*-dimethylaminophthalic anhydride (**DMAP**).[24, 33] Here, **DMAP** was coupled with cysteamine to generate probe 1. Probe 2, using glycine as a precursor, was generated to compare interactions with a non-thiol based metal binding group. To facilitate potential active-site hydrogen bonding interactions, we also synthesized cysteine-containing probes incorporating both the thiol and carboxylate moieties. Probes 3D and 3L were synthesized by combining D- or L-cysteine precursors with **DMAP** in refluxing acetic acid. Lastly, the methyl esters of 3D/3L were synthesized by reacting 3D/3L with thionyl chloride in methanol to afford 4D/4L in 68% and 50% yields, respectively. In some cases, when disulfide formation was ob-

served *via* LCMS, the crude mixture was reacted with 3 equivalents of *tris*(2-carboxyethyl)phosphine (TCEP) to generate the thiol and then purified *via* reverse phase chromatography. The probes were characterized for purity using ^{1}H-NMR, ^{13}C-NMR, and HRMS. All the probes displayed similar spectroscopic characteristics with λ_{ex} = 417-420 nm and λ_{em} = 575-580 nm in HEPES buffer. The quantum yields and extinction coefficients of probes **1-4L** in methanol are provided in Table S1.

Fluorescence response and inhibition of NDM-1 with probes 3D and 4D. Fluorescence spectroscopy studies of probes **1-4L** following incubation with NDM-1 (Fig. 1C) were performed in aqueous buffer supplemented with 10 μM ZnSO$_4$. Probes **1** and **2** displayed 6-fold and 1.2-fold fluorescence turn-on, respectively with NDM-1, indicating that that the thiol group in probe **1** is important for interaction with NDM-1, as has been reported previously.[1, 34] The cysteine derivatives, **3D** and **3L** displayed up to 15-fold and 11-fold turn-on respectively upon addition of NDM-1. These increases in fluorescence are accompanied by a 33 nm (**3D**) and 31 nm (**3L**) hypsochromic shift in λ_{em} from 575 nm (Fig S1). The cysteine methyl ester derivatives, **4D** and **4L**, showed 12-fold and 6-fold turn-on in fluorescence with NDM-1, respectively, along with 50 nm and 58 nm hypsochromic shifts in λ_{em} from 575 nm. The differences in turn-on and hypsochromic shifts between the two enantiomers indicates differences in interactions between these isomers and NDM-1. Amongst the 4 probes, **4L** showed the highest shift in λ_{em} followed by **4D**, indicating that the ester-based probes experience more hydrophobic interactions with non-polar regions of the NDM-1 active site compared to **3D/3L**. The larger turn-on for the D-forms (**3D**, **4D**) indicate differences in binding and fluorescence response, which are attributed to multiple factors including polarity, electrostatics, and sterics (Fig. S2). Preference of NDM-1 for one isomer over another is precedented. The well-studied NDM-1 inhibitor captopril shows differences in IC$_{50}$ values between its isomers with the D-form having a stronger interaction with NDM-1 (IC$_{50}$ D-captopril: 7.9 μM versus L-captopril: 202 μM).[7] We hypothesize that similar to D-captopril, the thiol group in **3D/4D** likely serves as a bridging ligand between Zn1 and Zn2 and the carboxylate/ester group facilitates binding through secondary interactions with the active site binding pocket, further stabilizing the probe:NDM-1 interaction. We measured an IC$_{50}$ of 6.3 ± 0.2 μM for probe **4D** and NDM-1 (Fig S3). The IC$_{50}$ value for **4D** is similar in magnitude to that of D-captopril and previously reported thiol-containing NDM-1 inhibitors.[31] Assuming competitive inhibition and fixing the substrate (chromacef)[35] concentration (20 μM; K_m = 0.66 ± 0.20 μM[35]), a K_i of 200 ± 30 nM can be calculated for the **4D**:dizinc NDM-1 interaction.[36] Despite structural similarity to **4D**, the probe **3D** did not fully abrogate activity (Fig S3), indicating likely differences in the binding interactions made between NDM-1 and **3D** and **4D**.

To better understand the differences between NDM-1 binding interactions with **3D**, **4D**, and L-captopril, we conducted computational simulations using a QM/DMD

method[37-39] (Fig. 2, Fig. S4, and SI). These simulations assessed different potential binding modes between the probes and NDM-1. The calculated binding mode for both **3D** and **4D** places the thiol group as a bridging Zn1 and Zn2 ligand, similar to that reported with L-captopril from crystal structures.[6] The lowest energy exemplary structure for bound **4D** demonstrates this conformation and is shown in Fig. 2. This pose reflects hydrophobic interactions made between the fluorophore end and a methionine residue (M34) in the substrate-binding β-hairpin loop of NDM-1 which may contribute to the fluorescence response of this probe (Fig. 2A). The calculated probe binding penalty is larger for **3D** (10.5 kcal/mol) than **4D** (4.2 kcal/mol), though both are smaller than the value calculated for L-captopril (19.5 kcal/mol) based on its crystal structure (PDB ID: 4EXS).[6] This result predicts that **4D** is less readily unbound and solvated than **3D** or L-captopril, and therefore binds more tightly to the NDM-1 active site, consistent with the lower measured IC$_{50}$ value. This difference in affinity likely arises from a stronger binding of the probe to the metals due to a better geometry and more favorable active site interactions. Calculated metal angle variances, which are a measure of unfavorable deviations of the Zn coordination from the ideal tetrahedral (Table 1) show that the lowest energy structure for **3D** reports a somewhat larger deviation from the ideal zinc tetrahedral geometry at 7.96° versus 7.52° for **4D**, contributing to poorer binding of **3D**. Assessment of the average metal angle variance across the full ensemble of states shows a larger difference of 10.77 ± 1.73° versus 8.32 ± 1.10°, with **3D** metal geometry being typically much worse than **4D**. Figs. 2B and 2C show hydrogen bonding
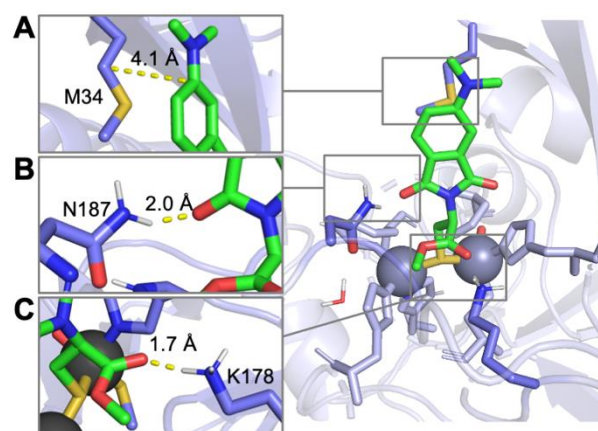

Figure 2. Proposed binding modes from QM/DMD simulations for probe **4D** with NDM-1 (PDB: 4EXS) with insets showing (A) interactions between the fluorophore end of the probe and hydrophobic M34 in Loop 3. (B) Interaction between N187 and the carbonyl oxygen of the imide ring of the fluorophore. (C) Interaction between K178 and the carbonyl groups in the metal binding group end of the probe.

interactions between asparagine (Asn 187) and lysine (Lys 178) residues and the carbonyl groups within the fluorophore and metal binding group of the probe, respectively. While the length of these hydrogen bonding interactions are similar between the lowest energy structures for **3D**

and **4D**, analysis of the full ensemble of states shows that a direct probe:Lys 178 hydrogen bond occurs about 38% more often in **4D** than **3D**. A more thorough discussion of these analyses and graphs of the full ensembles of states can be found in the SI. Based on *in vitro* spectroscopy, IC_{50} determinations, and computational studies indicating the probes' likely conformations, we decided to employ **4D** for all studies hereafter.

Table 1. Minimum values for binding penalties, metal angle variances, and distances for probes 3D and 4D.

Probe	Minimum values		Distances (Angstroms)			
	Binding penalties (kcal/mol)	Metal angle variance (degrees)	(thiol) S-Zn1	(thiol) S-Zn2	(carboxyl) O-NH (K178)	(carbonyl) O-NH (N187)
3D	10.5	7.96	2.3	2.4	1.8	2.5
4D	4.2	7.52	2.3	2.4	1.7	2.0

[†]We employed lowest binding energy mode 2 of the QM/DMD model for these data.

Reversibility and selectivity profile of probe 4D. We next studied the effect of $ZnSO_4$ and chelators on the fluorescence response between **4D** and NDM-1. Addition of up to 50 µM $ZnSO_4$ to **4D** and purified NDM-1 *in vitro* led to an increase in fluorescence turn-on to give an overall ~17-fold response (Fig. 3B). This result indicates that binding of **4D** to dizinc NDM-1 give the largest signal and suggests that the estimated $K_{d,Zn2}$ may be impacted by the other ligands present during each experiment (*e.g.,* ampicillin during prior K_{dZn2} estimates[8] and **4D** in our studies). Further, this indicates that more exogenous zinc is required under these conditions to fully metallate dizinc NDM-1 since at lower zinc supplementation (10 µM), the fluorescence response was lower. In contrast, incubation of **4D** with monozinc-NDM-1, formed *via* pre-treatment with 4-(2-pyridylazo)resorcinol (PAR),[5] led to a 70% reduction in observed fluorescence intensity relative to the same sample without PAR treatment or zinc supplementation, indicating that occupancy of the weaker binding Zn2 site is essential for the large fluorescence increase of 4D upon binding (Fig S5). Based on these results, we conclude that probe **4D** can be employed to specifically detect the holo dizinc-NDM-1 metalloform *in vitro*.

Next, to test the ability of **4D** to detect dynamic changes to NDM-1 metallation state or active-site occupancy, we performed several challenge studies. Treatments of the fluorescent **4D**:NDM-1 complex with the competitive inhibitor DL-captopril, the zinc chelator N,N,N′,N′-*tetrakis*(2-pyridinylmethyl)-1,2-ethanediamine (TPEN), and the inhibitor dipicolinic acid (DPA) (which has an inhibition mechanism that includes both NDM binding and zinc sequestration[35] all resulted in a decrease in observed fluorescence (Fig. 3A and 3B). With DL-captopril (200 µM), we observed the fluorescence turn-on decrease from the 17-fold maximum to ~13-fold (Fig. 3B). This par-

tial decrease is consistent with the fact that probe **4D** has a weaker affinity for NDM-1 than does the DL-captopril mixture and only partially displaces **4D** from the active site. Treatment with DPA (150 µM, $IC_{50, NDM-1}$=1.8 µM)[40] resulted in a similar decrease in fluorescence turn-on to 13-fold (Fig. 3B), again consistent with stronger affinity of DPA for NDM-1. Lastly, with the addition of the zinc chelator TPEN (50 µM) to the **4D**:NDM-1 complex (now in 10 µM $ZnSO_4$ to not overwhelm the chelator), we observed the fluorescence turn-on decrease from 12-fold to 9.2-fold (Fig. 3B). TPEN (Zn^{2+} K_d = 10^{-16} M;[41] $IC_{50, NDM-1}$ 0.088 µM[40]) can cause demetallation of NDM-1, and was expected to result in loss of probe binding, which is observed via a decreased fluorescence turn-on. The lack of complete fluorescence turn-on loss may be due to the inability of TPEN to access the active site when the probe is bound or to slow demetallation kinetics. Reduction in fluorescence following the chelation of zinc suggests that the probe (**4D**) can report on the availability of the holo dizinc NDM-1 metal site and can be used as either a probe to detect competitive ligand binding or to detect changes in metallation state.

To test probe selectivity, **4D** was incubated with other proteins including bovine and human carbonic anhydrase II (bCAII, hCAII), myoglobin, Cu,Zn-Superoxide dismutase (Cu,Zn-SOD), and bovine serum albumin (BSA). A small fluorescence turn-on (4-5-fold) with hCAII and BSA was observed (Fig. 3C). The fluorescence of **4D** was quenched when combined with myoglobin. Selectivity studies with another zinc metalloprotein carboxypeptidase A (CPA) at 2 µM concentrations showed no significant increase in fluorescence turn-on between **4D** and CPA. BSA is known to interact strongly with probes containing carboxylic groups.[42-43] Consistent with this trend, the carboxylate-containing probe **3D** gave up to an 85-fold increase in fluorescence when bound to BSA (data not shown), but the neutral ester-containing probe **4D** only showed a minimal 3-fold increase (Fig. 3C). This panel of representative metalloproteins indicates no obvious off-targets for **4D**.

Next, we tested **4D** with purified forms of two clinically significant metallo-β-lactamases that share 20-30% sequence identity to NDM-1: VIM-2 and IMP-1. VIM-2 and IMP-1, displayed 6-fold and 3.8-fold fluorescence turn-on, respectively, with probe **4D**. Despite low sequence identity, many metallo-β-lactamases have the conserved dizinc metal cluster and similar hydrophobic patches neighboring the active site, explaining the ability of **4D** to respond to these metalloenzymes. Differences in the surrounding sequence likely result in environments with less ability to enhance **4D** fluorescence than NDM-1. Addition of 50 µM $ZnSO_4$ to these incubations led to a minor increase in turn-on fluorescence (from 6-to 8-fold) for VIM-2 and a decrease to 3.5-fold for IMP-1. The small increase (or decrease) in fluorescence turn on observed with $ZnSO_4$ is consistent with the tighter Zn2 affinity of these enzymes.[44] [45]
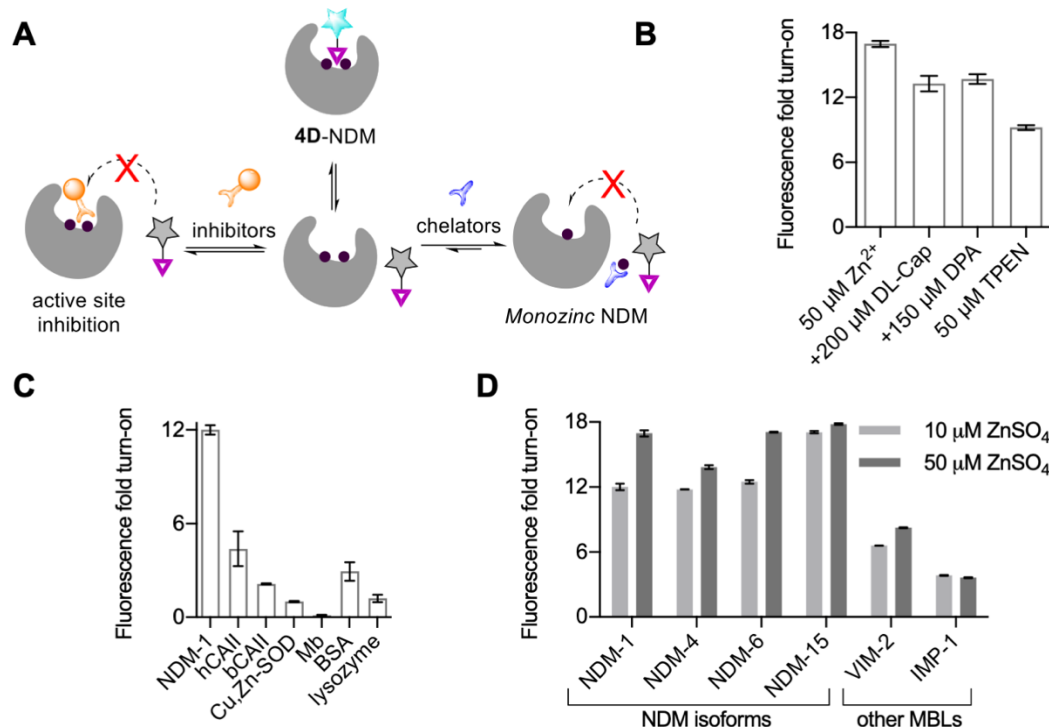
Figure 3. (A) Schematic showing effect of chelator and inhibitor treatment on **4D**/NDM-1 mixtures. (B) Change in fluorescence turn-on of **4D**-NDM-1 (1:3, 10 μM probe) following treatments with $ZnSO_4$, TPEN, DL-captopril (DL-Cap) and dipicolinic acid (DPA). (C) Fluorescence turn-on for **4D** with other proteins (1:3, 10 μM probe), human carbonic anhydrase II (hCAII), bovine carbonic anhydrase II (bCAII), Cu,Zn-superoxide dismutase (Cu,Zn-SOD), myoglobin (Mb), bovine serum albumin (BSA). (D) Fluorescence turn-on for **4D** with different NDM-1 isoforms and two other metallo-β-lactamases, VIM-2 and IMP-1 (1:3, 10 μM probe) in the presence of 10 μM $ZnSO_4$ (light grey) and 50 μM $ZnSO_4$ (dark grey).

Many clinical variants of NDM-1 appear to have evolved in response to zinc deprivation[8-10] We compared four purified NDM variants with differing Zn2 affinity for characterization with **4D**: NDM-1 (reference sequence, $K_{d,Zn2}$ =1 μM), NDM-4 (M154L, $K_{d,Zn2}$ = 230 nM), NDM-6 (A233V, $K_{d,Zn2}$ = 310 nM), and NDM-15 (M154L, A233V, $K_{d,Zn2}$ = 120 nM).[8] Each of these mutations are distant from the dizinc cluster and not likely to directly perturb the hydrophobic character of the active site. NDM-4 and NDM-6 showed 12 and 13-fold fluorescence turn-on, and like NDM-1, the turn-on increased with addition of more exogenous zinc. The results of NDM-15 contrast with those of the other variants and yielded the highest fluorescence turn-on of 17-fold (Fig. 3D), which only increased to 17.8-fold upon addition of 50 μM $ZnSO_4$. These results are consistent with the selectivity of probe **4D** specifically for the holo dizinc metalloform of NDM, which is more favored in the NDM-15 variant due to increased Zn2 affinity. Overall, these results indicate that fluorescence turn-on of **4D** is dependent on the NDM active site being fully metallated, at which point we observe ~ 17-18 fold fluorescence turn-on, indicating the usefulness of **4D** to monitor the dynamic metallation status of NDM.

Application of 4D in cells and cell lysates. Building on these *in vitro* studies, we characterized **4D**:NDM-1 interactions in live bacteria via confocal microscopy and in cell lysates via in-gel fluorescence staining using native SDS PAGE.[24] As seen in Fig 4A, BL21 (DE3) *E. coli* cells expressing Δ35 NDM-1 (see description of this construct below), bearing an *N*-terminal pelB leader sequence to direct periplasmic sorting, exhibits bright fluorescence staining when incubated with **4D**. Conversely, no fluorescence is observed in the absence of IPTG when NDM-1 is not expressed. These results are consistent with the association of **4D** turn-on fluorescence with the expression of periplasmically-directed NDM and consistent with the bioavailability of **4D** to proteins within the bacteria (presumably the periplasmic space). We observed a single fluorescent band in native SDS PAGE of cell lysates from NDM-1 expressing cells containing **4D** (Fig. 4B). (The running buffer for this native-SDS PAGE gel contains 0.01% SDS to aid resolution.) These results indicate that one major protein band is visualized using **4D,** and the mobility of this band corresponds with purified NDM, demonstrating selectivity of the probe for NDM in these cells under these conditions.
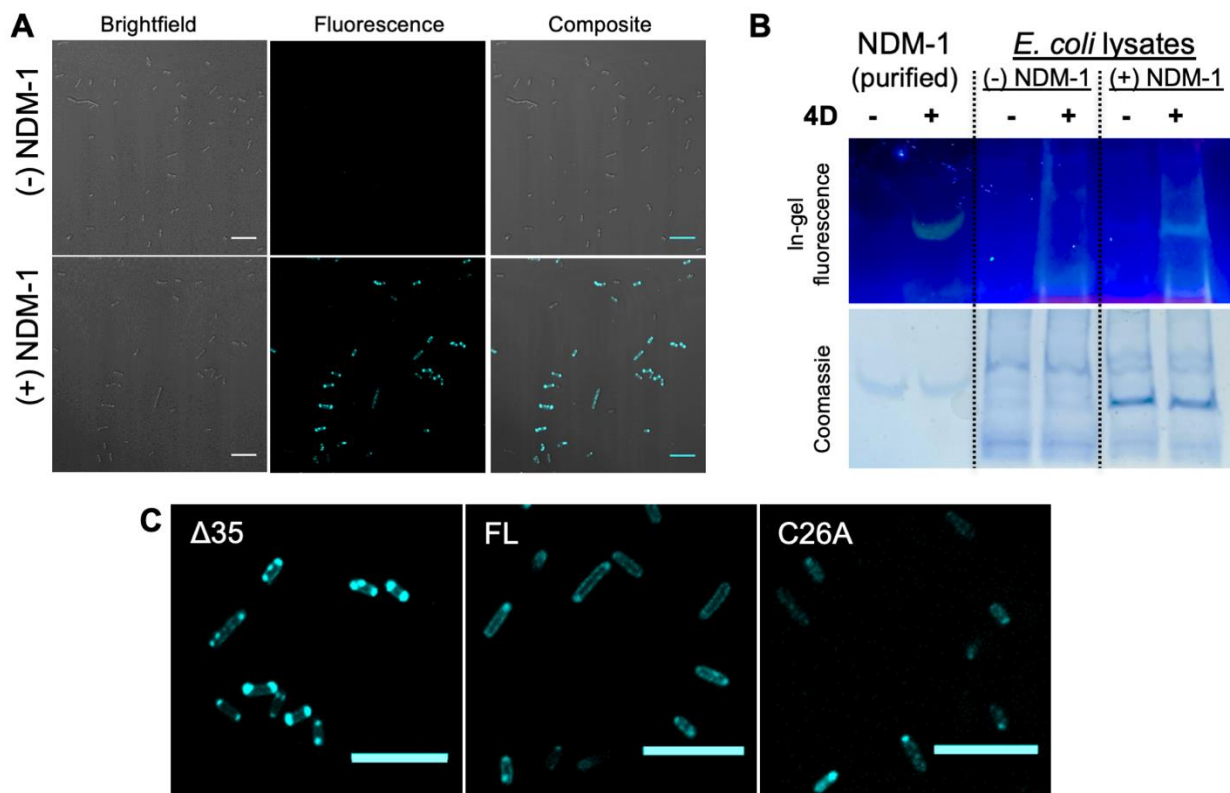
Figure 4. (A) Confocal fluorescence images of **4D** treated BL21 cells with the Δ35 construct in the presence and absence of IPTG for NDM-1 expression. (B) In-gel fluorescence (probe **4D**) and Coomassie staining of native SDS PAGE run at 120V for 40 mins (4-20% gel) with lysates of BL21 (DE3) cells with the Δ35 construct with and without NDM-1 expression. (C) Confocal fluorescence images of BL21 expressing different NDM-1 constructs (Δ35, FL, C26A) stained with **4D** (10 μM). For all imaging experiments, cells were grown in LB broth at 37°C, supplemented with 0.5 mM IPTG and 50 μM $ZnSO_4$ and protein expression induced for 2 hrs. Prior to imaging, the cells were re-suspended in M9 minimal media to obtain a final OD of ~0.3 for imaging. (Scale: 10 μm; $\lambda_{ex}/\lambda_{em}$: 405/ 486-614).

We note that as a control, we incubated mammalian cells (MCF-7) with **4D** and observed staining throughout the intracellular milieu (Fig. S6) indicating that this probe is not selective for NDM-1 in this context.

Three types of NDM-1 constructs were cloned into a pET-27b host vector after an IPTG-inducible T7 promoter, and assessed for their interactions with **4D** in *E. coli.* . Full length NDM-1 (FL) includes the native *N*-terminal leader sequence containing the periplasmic signal peptide and a lipidation signal as well as a *C*-terminal His₆-affinity tag.[5] This lipidation localizes NDM-1 to the inner leaflet of the outer membrane, placing the NDM catalytic domain within the periplasmic space.[11] C26A NDM-1 (C26A) is encoded by the same construct as FL but the Cys targeted for lipidation is mutated to an Ala to prevent modification. This mutation leads to accumulation of water soluble C26A NDM-1 in the periplasmic space.[11] Δ35 NDM-1 contains a 35 amino acid *N*-terminal truncation used to generate a water-soluble form of NDM used in our *in vitro* studies and is preceded by a pelB leader sequence to direct export to the periplasm followed by a Strep-tag II affinity tag that precedes the NDM sequence.[5]

After treatment of *E. coli* expressing FL NDM-1 with **4D**, confocal fluorescence microscopy was used to visualize fluorescence around the cell periphery, consistent with the expected periplasmic localization of the enzyme. This observation is similar to immunostained images of FL NDM-1 previously reported,[11] although the use of **4D** now enables dynamic imaging (see below). After long incubation times (> 2h), some cells start displaying punctate fluorescence patterns at the poles of the cells. Similar patterns were reported previously with Cys-reactive covalent fluorescent probes of NDM-1 and were attributed to accumulation of aggregated proteins,[27, 46] although experiments described below are more consistent with these regions also containing active, folded, dizinc NDM. *E. coli* cells expressing the C26A NDM-1 construct showed a similar pattern after treatment with **4D**. However, the punctate features at the poles are more prominent, again similar to previously reported immunostained images of C26A expressing cells.[11] **4D** treatment of the strain expressing Δ35 NDM-1 showed even more fluorescence at the poles (Fig. 4C, Fig. S7), similar to that reported for covalent fluorescent probes of NDM-1.[27] Additional control studies (for example staining with the disulfide version of **4D**) are

included in the SI. In sum, all three NDM constructs produced enzymes that were able to be effectively visualized using the probe **4D**. We chose to focus on Δ35 NDM-1 for the remaining experiments because the activities of soluble NDM variants are more sensitive to zinc chelators than those of lipidated NDM, and we sought to monitor the construct with the widest range of accessible metallation states.

Visualizing the dynamic metallation state of NDM-1 in bacteria. To rule out the possibility that the observed fluorescence turn-on of **4D** arises merely from partitioning into hydrophobic regions of unfolded, aggregated proteins at the poles of the bacteria, we tested whether **4D** could be displaced by specific NDM-1 substrates and inhibitors. As shown in the schematic (Fig. 5A), we expected that high concentrations of a β-lactam substrate would temporarily displace the probe and lead to a decrease in fluorescence. As the substrate concentration is decreased by enzymatic hydrolysis to product, we expected that **4D** would be able to outcompete and re-bind to the active site of NDM-1, thereby leading to recovery of the fluorescent signal. As predicted, addition of excess cephalexin (1 mM; K_m = 5.6 μM; k_{cat}/K_m = 8.4 x 10^6 $M^{-1}s^{-1}$)[5] caused a brief reduction in fluorescence of Δ35 NDM-1 expressing BL21 (DE3) *E. coli*, followed by an increasing fluorescence to a value near that preceding addition of the substrate (Fig. 5B, C). Fig. 5C shows representative images of cells in this experiment, showing an obvious increase in intensity at the poles over time where most of the fluorescence is localized. The ability to monitor reversible changes in NDM active-site accessibility highlights a design feature of using a reversible probe rather than some previously employed covalent tagging reagents. These results also support our interpretation that the punctate accumulation of NDM at the poles of the cell contains active, folded, dizinc protein rather than only aggregated misfolded proteins. Although the probe was designed to probe metallation state, we also recognize its ability to validate target engagement by NDM ligands in the cell. To further test this application, we used **4D** as a reporter to monitor target engagement by the inhibitor DL-captopril.

Above, we demonstrated the ability of DL-captopril to displace **4D** from NDM-1 *in vitro*. D-captopril has previously been shown to lower minimum inhibitor concentrations (MIC) of meropenem in NDM-1 expressing cells, so this compound can likely gain access to the periplasmic space.[47] To demonstrate that **4D** can report on target engagement by this inhibitor in cells, we treated Δ35 NDM-1

expressing BL21 (DE3) *E. coli* with **4D** and then with increasing concentrations of DL-captopril. The resulting fluorescence intensity decreased in a dose-dependent manner, indicating this NDM inhibitor can effectively compete with **4D** for binding.

To apply **4D** as a probe of NDM metallation status in *E. coli*, we studied the differential effects of three types of metal chelators on observed fluorescence: DPA, TPEN, and CaEDTA. Treatment by DPA requires approx. 200 μM to achieve a 50% decrease in fluorescence, with the decrease presumably representing a combination of displacing the **4D** from the active site and zinc sequestration (see above regarding the inhibition mechanism of DPA). This required concentration is much larger than the IC$_{50}$ of DPA for purified NDM-1 (0.5 μM),[35] indicating that bioavailability of DPA or competition with exogenous metal ions decrease its ability to impact NDM in *E. coli*. Accordingly, DPA is known to weakly chelate a wide range of divalent metal ions[48] that are present in cells and imaging media (10^{-2} to 10^{-7} M). We then monitored the effect of the membrane permeable, strong zinc chelator ($K_{d, Zn(II)}$ = 10^{-16} M)[41] TPEN (10 and 50 μM) over 15-20 mins. With 10 μM TPEN treatment, we observed a large concentration-dependent change in fluorescence intensity that decreased by ~66% with 10 μM TPEN under the assay conditions (Fig. 5F). TPEN does not resemble NDM-1 inhibitors and likely acts here solely as a zinc sequestration agent. Removal of the weaker affinity Zn2 either through direct interaction or by sequestration of the Zn2 after dissociation would be sufficient to decrease fluorescence by preventing formation of the **4D**:NDM complex, which exists in dynamic equilibrium with each of these metalloforms. Finally, we mimicked external zinc sequestration by using an extracellular zinc chelator[49] calcium EDTA (CaEDTA). Addition of 10 μM CaEDTA ($K_{d, Zn(II)}$ = 10^{-9} M)[49] showed no significant decrease in fluorescence (Fig. 5G). However, higher CaEDTA concentrations (50 μM), decreased fluorescence intensity by ~33%. A number of reports have indicated increased susceptibility of NDM-1 expressing *E. coli* to antibiotics upon treatment with EDTA (for one example ref[8]). However, EDTA can increase outer membrane permeability,[50] so it is not entirely clear whether the increases in susceptibility are due to zinc sequestration or by increasing periplasmic access. Here, we use the probe **4D** to demonstrate that NDM-1 is demetallated by treatment with exogenous zinc chelators, supporting zinc sequestration as the likely mechanism for increased susceptibility.
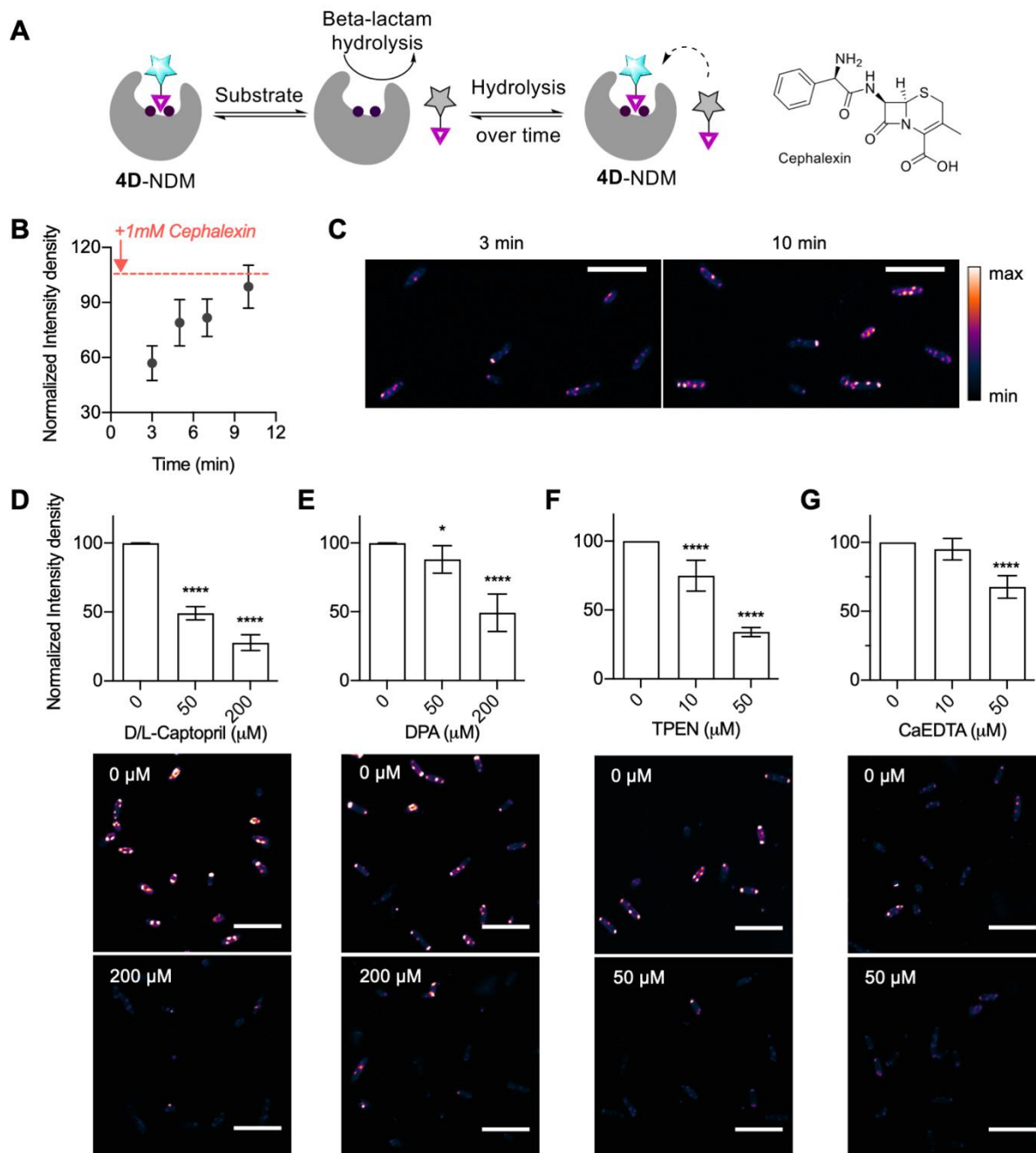
Figure 5. (A) Schematic showing probe displacement by the substrate and the structure of cephalexin (B) Time-dependent fluorescence intensity after addition of cephalexin (1 mM) to **4D** treated *E. coli* BL21 (DE3) expressing Δ35 NDM-1) (C) Example images from 3 min versus 10 min samples used to construct panel B. Effect of DL-captopril (panel D), DPA (panel E), TPEN (panel F) and CaEDTA (panel G) on the fluorescence intensity of BL21 (DE3) cells expressing Δ35 NDM-1 after 20 min incubation (5 min with 8μM **4D** followed by 15 mins of treatment with indicated additives). All data were recorded in triplicate and analyzed using two-way ANOVA (* $p < 0.05$, ** $p < 0.01$, *** $p < 0.001$, **** $p < 0.0001$). Scale bar 10 μm. $\lambda_{ex}/\lambda_{em}$ 405/ 486-614.

Comparing metalation status between clinical variants of NDM. Since the discovery of NDM in 2008, more than 30 allelic variants of NDM have emerged (accessed Dec 17, 2020).[51] While many of these variants do not show appreciably improved kinetic constants for β-lactam hydrolysis or resistance to inhibitors, a large proportion of the variants have lower $K_{d,Zn2}$ values and an associated increase in thermostability.[8-10, 52] NDM variants with in-

creased Zn2 affinity can outcompete other variants when grown in environments with low zinc availability.[8-10] NDM-15 has one of the most improved $K_{d,Zn2}$ values characterized to date.[8] We compared the ability of probe **4D** to visualize Δ35 NDM-1 and the variant Δ35 NDM-15 when expressed and exported to the periplasm of *E. coli*. The localization of Δ35 NDM-15 was similar to that of Δ35 NDM-1, but showed more fluorescence around the cell

periphery (Fig. 6A), consistent with less trapping of this variant within unfolded proteins at the poles, which is also consistent with the increased thermostability of this variant.[8, 10, 52] Despite these similarities, challenges of these strains by zinc chelators showed marked differences. Treatment with TPEN and DPA resulted in markedly smaller changes in fluorescence intensity for NDM-15 than NDM-1 (Fig. 6B). TPEN, a stronger zinc chelator only decreased the fluorescence by ~30% at 50 µM concentration. DPA treatment had no effect on fluorescence, even at 200 µM. The probe **4D** clearly indicates that NDM-15 is more resistant to the rapid demetallation observed with NDM-1, even to membrane permeable chelators.
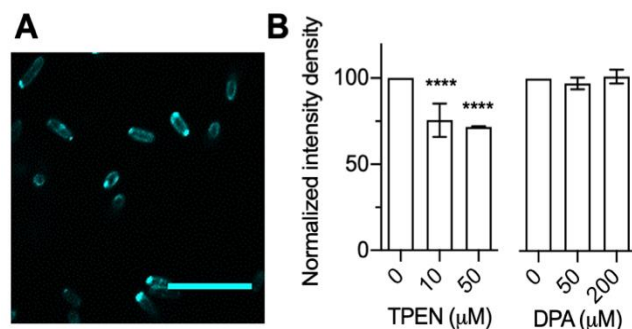

Figure 6. (A) Fluorescence image showing expression and localization of NDM-15 cellular Δ35 construct with probe **4D**. (B) Effect of addition of TPEN and DPA to NDM-15 Δ35 BL21 cells. All data were recorded in triplicate (2-3 different trials) and two-way ANOVA was performed to determine significance (**** p <0.0001). Scale bar 10 µm; $\lambda_{ex}/\lambda_{em}$ 405/486-614.

CONCLUSIONS

We report the development of a novel probe, **4D**, to monitor the dynamic metallation state of NDM within *E. coli*. Coupling of an environment-sensitive fluorophore to a thiol-based NDM inhibitor scaffold resulted in an active-site directed ligand with a K_i of 200 nM that achieves a 17-fold fluorescence turn-on upon binding NDM-1. Molecular modeling is consistent with a binding conformation in which the probe's thiolate bridges the two zincs at the active site metal cluster of NDM-1 while the inhibitor's fluorophore makes interactions with hydrophobic residues in the neighboring substrate-binding β-hairpin loop. Binding of the probe is reversible - it can be displaced either by competition with non-fluorescent active-site ligands or by demetallation of NDM, with the resulting loss in fluorescence enabling monitoring of dynamic alterations to the active site metal content. The probe is shown to be selective for NDM using a small panel of potential off-target metalloproteins and by fluorescence imaging of native gel electrophoresis gels of cell lysates. Notably, the probe can be used with confocal microscopy to image dizinc NDM expressed in the *E. coli* periplasm and can report on dynamic changes in ligand binding during substrate and inhibitor engagement with NDM as well as during demetallation by both cell-permeable and cell-impermeable zinc chelators. In comparison with NDM-1, expression of the clinical variant NDM-15 is

shown to be more resistant to demetallation by zinc chelators than NDM-1, consistent with decreases in antibiotic susceptibility when resistant strains are grown under similar conditions. These experiments establish **4D** as a useful probe for dynamically monitoring NDM metallation state and active-site occupancy in bacteria during the study of metal ion sequestration in host-pathogen interactions, evolution of more resistant enzyme variants, and the development of novel NDM-directed therapeutics to counter the rising threat of carbapenem resistant Enterobacteriaceae. This novel imaging tool can be particularly useful for screening new inhibitors for NDM and ascertaining efficacy of target engagement *in vivo*.

The bigger implications of these results can be seen in the importance of studying metallation status as a function of chelator treatment *in vitro* and *in vivo*. By developing an active site binding fluorescent probe for a targeted metalloprotein, that is reversible, selective, and cell permeable, we have been able to dynamically monitor the metallation status of zinc metalloproteins in question as well as their evolution in different systems. Previously, we studied the effects of cellular metal homeostasis perturbations on carbonic anhydrase (CA) in mammalian HeLa cells using a CA-binding fluorescence probe.[24] Treatments with 10 µM TPEN and 1 µM zinc pyrithione (ZnPT) to decrease and increase intracellular zinc availability, respectively, did not affect observed fluorescence associated with the fluorescent probe-CA complex. This result was consistent with *in vitro* studies where TPEN failed to affect the fluorescence of the probe-CA complex. We hypothesize that these results are mainly due to the structure of CA–a narrow and deep active site with high zinc affinity and thus, resistance to zinc demetallation by bulky chelators like TPEN. Even though TPEN's affinity for zinc (~10^{-16} M) is greater than that of CA (~10^{-12} M), the rigid, 15 Å deep and ~9-10 Å wide CA active site lined by multiple hydrophobic and hydrophilic moieties likely makes it difficult for TPEN to approach and remove Zn^{2+} from CA. Additionally, the results from cellular studies with ZnPT indicate that CA generally exists in a fully metallated form in the cell. This result sheds light on how nature has chosen to adapt and preserve one of its most essential metalloproteins that plays important roles in respiration, pH balance, and transport of ions in cells. Its 15 isoforms have distinct functions and localizations in the mammalian cell and thus, it is highly likely that this protein has evolved over a long period of time to optimize its cellular functions.

In contrast, **4D** enabled us to observe the dynamic loss of NDM-1 metallation upon cell-impermeable chelator treatment. These experiments illustrate that, unlike CA, the periplasmic NDM-1 metallation state can be significantly affected by fluxes in zinc availability and that clinical variants (like NDM-15) have emerged that are less susceptible to these fluxes. The development of specific, reversible fluorescent probes to report on metallation status provide new tools to better understand the evolution of metalloproteins in response to different selective pressures.

ASSOCIATED CONTENT

Supporting Information. The synthetic procedures, materials and methods and supporting figures are included in the supporting information (SI). This material is available free of charge via the Internet at http://pubs.acs.org.

AUTHOR INFORMATION

Corresponding Author

* E.L.Q.: email, emilyque@cm.utexas.edu; telephone (512)471-4490, ORCID 0000-0001-6604-3052.
*W.F.: email, walt.fast@austin.utexas.edu; telephone (512) 232-4000, ORCID: 0000-0001-7567-2213.

Author Contributions

All authors have given approval to the final version of the manuscript. R.M., A.H. and D.T. synthesized and characterized the probes. D.D.R., P.W.T, A.C.S and Z.C. contributed towards cell constructs and protein purification. D.D.R. and R.M. contributed to cell growth, lysis and gel electrophoresis studies. R.M. contributed to confocal image acquisition and processing. D.J.R. and A.N.A. contributed computational modeling.

ABBREVIATIONS

NDM, New Delhi Metallo-β-lactamase; TCEP, *tris*(2-carboxyethyl)phosphine; TPEN, N,N,N′,N′-*tetrakis*(2-pyridinylmethyl)-1,2-ethanediamine; DPA, dipicolinic acid; PAR, 4-(2-pyridylazo)resorcinol; CA, carbonic anhydrase; MIC, minimum inhibitor concentrations; BSA, bovine serum albumin; ZnPT, zinc pyrithione.

REFERENCES

(1) Brem, J., et al. Structural Basis of Metallo-β-Lactamase Inhibition by Captopril Stereoisomers. *Antimicrob. Agents Chemother.* **2016,** *60,* 142.

(2) Dortet, L.; Poirel, L.; Nordmann, P. Worldwide dissemination of the NDM-type carbapenemases in Gram-negative bacteria. *Biomed. Res. Int.* **2014,** *2014,* 249856.

(3) Yong, D., et al. Characterization of a new metallo-beta-lactamase gene, bla(NDM-1), and a novel erythromycin esterase gene carried on a unique genetic structure in Klebsiella pneumoniae sequence type 14 from India. *Antimicrob. Agents Chemother.* **2009,** *53,* 5046.

(4) Sun, Z.; Hu, L.; Sankaran, B.; Prasad, B. V. V.; Palzkill, T. Differential active site requirements for NDM-1 β-lactamase hydrolysis of carbapenem versus penicillin and cephalosporin antibiotics. *Nat. Comm.* **2018,** *9,* 4524.

(5) Thomas, P. W., et al. Characterization of Purified New Delhi Metallo-β-lactamase-1. *Biochemistry* **2011,** *50,* 10102.

(6) King, D. T.; Worrall, L. J.; Gruninger, R.; Strynadka, N. C. New Delhi metallo-β-lactamase: structural insights into β-lactam recognition and inhibition. *J. Am. Chem. Soc.* **2012,** *134,* 11362.

(7) Guo, Y., et al. A structural view of the antibiotic degradation enzyme NDM-1 from a superbug. *Protein & Cell* **2011,** *2,* 384.

(8) Cheng, Z., et al. Evolution of New Delhi metallo-β-lactamase (NDM) in the clinic: Effects of NDM mutations on stability, zinc affinity, and mono-zinc activity. *J. Biol. Chem.* **2018,** *293,* 12606.

(9) Stewart, A. C., et al. Clinical Variants of New Delhi Metallo-β-Lactamase Are Evolving To Overcome Zinc Scarcity. *ACS Infect. Dis.* **2017,** *3,* 927.

(10) Bahr, G.; Vitor-Horen, L.; Bethel, C. R.; Bonomo, R. A.; González, L. J.; Vila, A. J. Clinical Evolution of New Delhi Metallo-β-Lactamase (NDM) Optimizes Resistance under Zn(II) Deprivation. *Antimicrob. Agents Chemother.* **2018,** *62.*

(11) González, L. J.; Bahr, G.; Nakashige, T. G.; Nolan, E. M.; Bonomo, R. A.; Vila, A. J. Membrane anchoring stabilizes and favors secretion of New Delhi metallo-β-lactamase. *Nat. Chem. Biol.* **2016,** *12,* 516.

(12) Falconer, S. B., et al. Zinc Chelation by a Small-Molecule Adjuvant Potentiates Meropenem Activity in Vivo against NDM-1-Producing Klebsiella pneumoniae. *ACS Infect. Dis.* **2015,** *1,* 533.

(13) Worthington, R. J.; Melander, C. Combination approaches to combat multidrug-resistant bacteria. *Trends. Biotechnol.* **2013,** *31,* 177.

(14) Becker, K. W.; Skaar, E. P. Metal limitation and toxicity at the interface between host and pathogen. *FEMS Microbiol. Rev.* **2014,** *38,* 1235.

(15) Hood, M. I.; Skaar, E. P. Nutritional immunity: transition metals at the pathogen-host interface. *Nat. Rev. Microbiol.* **2012,** *10,* 525.

(16) Wątły, J.; Potocki, S.; Rowińska-Żyrek, M. Zinc Homeostasis at the Bacteria/Host Interface-From Coordination Chemistry to Nutritional Immunity. *Chemistry* **2016,** *22,* 15992.

(17) Begg, S. L. The role of metal ions in the virulence and viability of bacterial pathogens. *Biochem. Soc. Trans.* **2019,** *47,* 77.

(18) Hu, Z.; Gunasekera, T. S.; Spadafora, L.; Bennett, B.; Crowder, M. W. Metal content of metallo-beta-lactamase L1 is determined by the bioavailability of metal ions. *Biochemistry* **2008,** *47,* 7947.

(19) Meini, M. R.; González, L. J.; Vila, A. J. Antibiotic resistance in Zn(II)-deficient environments: metallo-β-lactamase activation in the periplasm. *Future Microbiol.* **2013,** *8,* 947.

(20) Wang, J., et al. Multi-metal Restriction by Calprotectin Impacts De Novo Flavin Biosynthesis in Acinetobacter baumannii. *Cell Chem. Biol.* **2019,** *26,* 745.

(21) Chan, A. N.; Shiver, A. L.; Wever, W. J.; Razvi, S. Z.; Traxler, M. F.; Li, B. Role for dithiolopyrrolones in disrupting bacterial metal homeostasis. *Proc. Natl. Acad. Sci. U.S.A.* **2017,** *114,* 2717.

(22) Zygiel, E. M.; Nolan, E. M. Transition Metal Sequestration by the Host-Defense Protein Calprotectin. *Annu. Rev. Biochem.* **2018,** *87,* 621.

(23) Siemann, S.; Brewer, D.; Clarke, A. J.; Dmitrienko, G. I.; Lajoie, G.; Viswanatha, T. IMP-1 metallo-beta-lactamase: effect of chelators and assessment of metal requirement by electrospray mass spectrometry. *Biochim. Biophys. Acta* **2002,** *1571,* 190.

(24) Mehta, R., et al. A new probe for detecting zinc-bound carbonic anhydrase in cell lysates and cells. *Chem. Commun.* **2018,** *54,* 5442.

(25) Mao, W.; Wang, Y.; Qian, X.; Xia, L.; Xie, H. A Carbapenem-Based Off–On Fluorescent Probe for Specific Detection of Metallo-β-Lactamase Activities. *ChemBioChem* **2019**, *20*, 511.

(26) Kim, J., et al. Development of carbapenem-based fluorogenic probes for the clinical screening of carbapenemase-producing bacteria. *Bioorg. Chem.* **2020**, *94*, 103405.

(27) Chen, C., et al. A protein structure-guided covalent scaffold selectively targets the B1 and B2 subclass metallo-β-lactamases. *Chem. Commun.* **2018**, *54*, 4802.

(28) Singha, M., et al. Rapid Fluorescent-Based Detection of New Delhi Metallo-β-Lactamases by Photo-Cross-Linking Using Conjugates of Azidonaphthalimide and Zinc(II)-Chelating Motifs. *ACS Omega* **2019**, *4*, 10891.

(29) Brem, J., et al. Structural Basis of Metallo-β-Lactamase Inhibition by Captopril Stereoisomers. *Antimicrobial Agents and Chemotherapy* **2016**, *60*, 142.

(30) Yusof, Y.; Tan, D. T. C.; Arjomandi, O. K.; Schenk, G.; McGeary, R. P. Captopril analogues as metallo-β-lactamase inhibitors. *Bioorg. Med. Chem. Lett.* **2016**, *26*, 1589.

(31) Cui-Gai, B.; Yin-Tong, X.; Ning-Ning, L.; Jing-Han, W.; Cheng, Y.; Yue Chen and Hong-Gang, Z. Cysteine and Its Derivatives as New Delhi Metallo-beta-lactamase-1 Inhibitors. *Curr. Enzyme Inhibit.* **2015**, *11*, 46.

(32) Sainlos, M.; Imperiali, B. Synthesis of anhydride precursors of the environment-sensitive fluorophores 4-DMAP and 6-DMN. *Nat. Protoc.* **2007**, *2*, 3219.

(33) Vázquez, M. E.; Blanco, J. B.; Imperiali, B. Photophysics and biological applications of the environment-sensitive fluorophore 6-N,N-dimethylamino-2,3-naphthalimide. *J. Am. Chem. Soc.* **2005**, *127*, 1300.

(34) Klingler, F. M., et al. Approved Drugs Containing Thiols as Inhibitors of Metallo-β-lactamases: Strategy To Combat Multidrug-Resistant Bacteria. *J. Med. Chem.* **2015**, *58*, 3626.

(35) Chen, A. Y., et al. Dipicolinic Acid Derivatives as Inhibitors of New Delhi Metallo-β-lactamase-1. *J. Med. Chem.* **2017**, *60*, 7267.

(36) Copeland, R. A. Evaluation of enzyme inhibitors in drug discovery. A guide for medicinal chemists and pharmacologists. *Methods Biochem. Anal.* **2005**, *46*, 1.

(37) Sparta, M.; Shirvanyants, D.; Ding, F.; Dokholyan, N. V.; Alexandrova, A. N. Hybrid dynamics simulation engine for metalloproteins. *Biophys. J.* **2012**, *103*, 767.

(38) Reilley, D. J., et al. Toxic and Physiological Metal Uptake and Release by Human Serum Transferrin. *Biophys. J.* **2020**, *118*, 2979.

(39) Nechay, M. R.; Gallup, N. M.; Morgenstern, A.; Smith, Q. A.; Eberhart, M. E.; Alexandrova, A. N. Histone Deacetylase 8: Characterization of Physiological Divalent Metal Catalysis. *J. Phys. Chem. B* **2016**, *120*, 5884.

(40) Jackson, A. C.; Zaengle-Barone, J. M.; Puccio, E. A.; Franz, K. J. A Cephalosporin Prochelator Inhibits New Delhi Metallo-β-lactamase 1 without Removing Zinc. *ACS Infect. Dis.* **2020**, *6*, 1264.

(41) Golovine, K.; Uzzo, R. G.; Makhov, P.; Crispen, P. L.; Kunkle, D.; Kolenko, V. M. Depletion of intracellular zinc increases expression of tumorigenic cytokines VEGF, IL-6 and IL-8 in prostate cancer cells via NF-κB dependent pathway. *Prostate* **2008**, *68*, 1443.

(42) Jeremias, H. F., et al. Study of the interactions of bovine serum albumin with a molybdenum(II) carbonyl complex by spectroscopic and molecular simulation methods. *PLOS ONE* **2018**, *13*, e0204624.

(43) Lee, S., et al. Development of Human Serum Albumin Selective Fluorescent Probe Using Thieno[3,2-b]pyridine-5(4H)-one Fluorophore Derivatives. *Sensors* **2019**, *19*, 5298.

(44) Aitha, M., et al. Biochemical, Mechanistic, and Spectroscopic Characterization of Metallo-β-lactamase VIM-2. *Biochemistry* **2014**, *53*, 7321.

(45) Yamaguchi, Y., et al. A Demetallation Method for IMP-1 Metallo-β-Lactamase with Restored Enzymatic Activity Upon Addition of Metal Ion(s). *ChemBioChem* **2011**, *12*, 1979.

(46) Rokney, A.; Shagan, M.; Kessel, M.; Smith, Y.; Rosenshine, I.; Oppenheim, A. B. E. coli transports aggregated proteins to the poles by a specific and energy-dependent process. *J. Mol. Biol.* **2009**, *392*, 589.

(47) Ma, G., et al. Structure-guided optimization of D-captopril for discovery of potent NDM-1 inhibitors. *Bioorg. Med. Chem.* **2020**, *29*, 115902.

(48) Chung, L.; Rajan, K. S.; Merdinger, E.; Grecz, N. Coordinative binding of divalent cations with ligands related to bacterial spores. Equilibrium studies. *Biophys. J.* **1971**, *11*, 469.

(49) Radford, R. J.; Lippard, S. J. Chelators for investigating zinc metalloneurochemistry. *Curr. Opin. Chem. Biol.* **2013**, *17*, 129.

(50) Vaara, M. Agents that increase the permeability of the outer membrane. *Microbiol. Rev.* **1992**, *56*, 395.

(51) https://http://www.ncbi.nlm.nih.gov/pathogens/refgene/ - gene_family:(blaNDM).

(52) Makena, A., et al. Biochemical characterization of New Delhi metallo-β-lactamase variants reveals differences in protein stability. *J. Antimicrob. Chemother.* **2015**, *70*, 463.

1
2
3
4
5
6
7
8
9
10
11
12
13
14
15
16
17
18
19
20
21
22
23
24
25
26
27
28
29
30
31
32
33
34
35
36
37
38
39
40
41
42
43
44
45
46
47
48
49
50
51
52
53
54
55
56
57
58
59
60

Authors are required to submit a graphic entry for the Table of Contents (TOC) that, in conjunction with the manuscript title, should give the reader a representative idea of one of the following: A key structure, reaction, equation, concept, or theorem, etc., that is discussed in the manuscript. Consult the journal's Instructions for Authors for TOC graphic specifications.

Insert Table of Contents artwork here